The Design of Measurement-Based Underwater Acoustic Channel Simulators Using the INLSA Algorithm

Meisam Naderi [1], Matthias Pätzold [1], and Alenka G. Zajić [2]
[1] *Faculty of Engineering and Science, University of Agder, P.O. Box 509, 4898 Grimstad, Norway*
[2] *School of Electrical and Computer Engineering, Georgia Institute of Technology, Atlanta, GA 30332-0280, USA*
Emails: [1]{meisam.naderi, matthias.paetzold}@uia.no, [2]alenka.zajic@ece.gatech.edu

***Abstract*—This paper utilizes the iterative nonlinear least square approximation (INLSA) algorithm for designing measurement-based wideband shallow underwater acoustic (UWA) channel simulators. Measurement-based channel simulators are essential for the test, optimization, and performance analysis of UWA communication systems. The aim is to fit the time-variant channel impulse response (TVCIR) of the simulation model to that of the measured UWA channel. The performance of the designed UWA channel simulator is assessed by comparing the time-frequency correlation function (TFCF), the power delay profile (PDP), and the probability density function (PDF) of the channel envelope with the corresponding quantities of the measured channel. The results of the assessment show an excellent match between the statistical properties of the UWA channel simulator, designed by the INLSA method, and those of the real-world UWA channel. It is also shown that the distribution of the channel envelope of our measurement data, which is collected from a shallow-water environment, follows closely the Rayleigh distribution.**

***Index terms* — Measurement-based channel modelling, shallow underwater acoustic channels, iterative optimization, underwater acoustic communications, wideband channels, power delay profile, time-frequency correlation function.**

I. INTRODUCTION

Underwater acoustic (UWA) communication systems have been receiving noticeable attention in the past decade. UWA networks have been studied in various areas due to their potential applications in oceanography. For the design, test, and performance analysis of UWA communication systems, realistic channel models are required. This calls for the statistical analysis of UWA channels in terms of correlation functions, distribution of the channel envelope, and power delay profiles (PDPs). For the performance analysis of UWA communication systems, one usually resorts to computer simulations, which provide a powerful means to assess the system performance. They can also be used to confirm the correctness of theoretical results obtained analytically.

Recently, some few reference models for UWA channel have been developed in [1]–[3], however, none of them can precisely capture all physical properties of UWA channels. For instance, a stochastic reference channel model for wideband MIMO mobile-to-mobile (M2M) UWA channels has been proposed in [1]. Therein, the reference model has been developed by combining the deterministic ray-tracing concept with statistical methods to account for the randomness of the propagation environment. In the absence of a standardized model for UWA channels, measurement-based channel modelling is an alternative approach to model the behaviour of real-world UWA channels. However, it is a scenario-specific approach. For the design of a measurement-based channel simulator, we need to estimate the model parameters, including the path gains, Doppler frequencies, propagation delays, and phase shifts. Hence, sophisticated and efficient parameter computation methods are required to precisely estimate these model parameters from real-world measurement data. In the literature, many powerful parameter computation methods have been proposed. For example, an application of the estimation of signal parameters via rotational invariance techniques (ESPRIT) algorithm to design a measurement-based wideband channel model is presented in [4]. The space-alternating generalized expectation-maximization (SAGE) algorithm is another parameter computation method, which is widely used because of its high performance [5]. Furthermore, the iterative nonlinear least square approximation (INLSA) algorithm has been proposed in [6] to design measurement-based wideband channel simulators. Therein, the authors showed that the INLSA algorithm has lower complexity and better performance compared with the SAGE algorithm. The INLSA has further been developed and refined in [7]–[9]. It has been shown in [10] that the INLSA outperforms the SAGE and ESPRIT algorithms with respect to their fitting accuracy to the autocorrelation function (ACF) of a given reference model.

There are numerous studies focussing on the modelling of UWA channels, which are based on measured acoustic channel data collected in specific scenarios. For example, the probability density function (PDF) of the UWA channel envelope has been shown to be Rayleigh distributed in [11], [12], while the authors of [13], [14] have reported that the envelope follows the Rice distribution. Besides these distributions, the channel envelope may also follow the lognormal distribution or the K-distribution as claimed in [15] and [16], respectively. These controversial studies demonstrate that there is a need for a realistic UWA channel simulator.

In this paper, we propose a sum-of-cisoids uncorrelated scattering (SOCUS) channel simulator based on shallow UWA measurement data. To obtain the experiment data, we launched

978-1-4799-8736-8/15/$31.00 ©2015 IEEE

a campaign to measure a shallow UWA channel. The measured data was used as a starting point for computing the TVCIR of the UWA channel. The objective is to design a channel simulator that emulates the TVCIR of the measured channel. Starting from the measurement-based channel simulator, we derive the time-variant channel transfer function (TVCTF), time-frequency correlation function (TFCF), PDP, and the channel envelope PDF. To determine the parameters of the simulation model, we employ the INLSA method developed in [9]. It needs to mention that the INLSA algorithm has not been applied to UWA communications. We will present a procedure that allows us to easily use it for the area of measurement-based UWA channel modelling. It will be shown that the INLSA algorithm estimates precisely the simulation model parameters and results in an excellent match to the statistical properties of real-world channels. Our numerical results show that a good fitting between the measured channel and the simulation model can be achieved with respect to the TVCIR, TFCF, PDP, and the channel envelope distribution.

The rest of this paper is organized as follows. In Section II, the wideband SOCUS channel simulation model is presented. Section III describes the utilized parameter computation method. Sections IV and V focus on the measurement scenario and the measurement results, respectively. The numerical results are illustrated in Section VI. Finally, the conclusions are drawn in Section VII.

II. The Wideband Channel Simulation Model

A measured UWA TVCIR $\check{h}(\tau', t)$ of a single snapshot measurement scenario is usually limited in the time domain and the delay domain. Given a measured UWA TVCIR $\check{h}(\tau', t)$, our aim is to develop a channel simulation model such that the statistical properties of the simulation model are as close as possible to those of the measured real-world channel.

A. TVCIR

In this section, we adopt a channel simulation model with TVCIR $\tilde{h}(\tau', t)$ based on the SOCUS model, which is an appropriate model for a large class of wideband measured channels under non-isotropic scattering conditions. The TVCIR $\tilde{h}(\tau', t)$ of the SOCUS model is given by [17, Eq. (7.138)]

$$\tilde{h}(\tau', t) = \sum_{l=0}^{L-1} \sum_{n=1}^{N_l} c_{n,l}\, e^{\,j(2\pi f_{n,l} t + \theta_{n,l})} \delta(\tau' - \tau_l') \tag{1}$$

where L stands for the number of propagation paths which experience different propagation delays τ_l'. It should be mentioned that the propagation delays τ_l' and the number of paths L are obtained directly from the measured data. The symbol N_l denotes the number of paths having the same propagation delay. The nth component of the lth path is characterized by its path gain $c_{n,l}$, Doppler frequency $f_{n,l}$, and phase shift $\theta_{n,l}$. Since the propagation delays τ_l' are achieved from the measured TVCIR $\check{h}(\tau', t)$, we need to determine the set of parameters $\mathcal{P} = \{N_l, c_{n,l}, f_{n,l}, \theta_{n,l}\}$. In this case, instead of computing the TVCIR $\tilde{h}(\tau', t)$, we compute the model parameters of the time-variant complex channel gains $\tilde{\mu}_l(t)$ having the form

$$\tilde{\mu}_l(t) = \sum_{n=1}^{N_l} \tilde{\mu}_{n,l}(t) = \sum_{n=1}^{N_l} c_{n,l}\, e^{\,j(2\pi f_{n,l} t + \theta_{n,l})} \tag{2}$$

where $\tilde{\mu}_{n,l}(t)$ denotes the complex channel gain of the nth path corresponding to the delay τ_l'.

B. TVCTF

To analyze the performance of the channel simulator, we need to compare the statistical properties of the channel simulator, such as the TFCF, PDP, and the channel envelope PDF with those of the measured channel. For the computation of the TFCF, we first need to derive the TVCTF $\tilde{H}(f', t)$, which is obtained by taking the Fourier transform of the TVCIR $\tilde{h}(\tau', t)$ with respect to propagation delays τ'. This results in

$$\tilde{H}(f', t) = \sum_{l=0}^{L-1} \sum_{n=1}^{N_l} \tilde{\mu}_{n,l}(t) e^{-j2\pi f' \tau_l'} = \sum_{l=0}^{L-1} \tilde{\mu}_l(t) e^{-j2\pi f' \tau_l'}. \tag{3}$$

C. TFCF

As discussed in the previous section, the TVCTF enables us to compute the TFCF. Under the assumption that the UWA channel simulator is wide-sense stationary in frequency f' and time t, the TFCF $\tilde{r}_{HH}(\nu', \tau)$ is given by [17, Eq. (7.145)]

$$\tilde{r}_{HH}(\nu', \tau) = \sum_{l=0}^{L-1} \sum_{n=1}^{N_l} c_{n,l}^2\, e^{\,j2\pi(f_{n,l}\tau - \nu' \tau_l')} \tag{4}$$

where the symbols ν' and τ denote the frequency and time separation variables, respectively.

D. PDP

The PDP $\tilde{p}_{\tau'}(\tau')$ of the SOCUS channel simulator can be expressed by [17, Eq. (7.151)]

$$\tilde{p}_{\tau'}(\tau') = \sum_{l=0}^{L-1} \sum_{n=1}^{N_l} c_{n,l}^2 \delta(\tau' - \tau_l'). \tag{5}$$

Note that the behavior of the PDP $\tilde{p}_{\tau'}(\tau')$ is fully determined by the model parameters L, N_l, $c_{n,l}$, and τ_l'. The average delay $\tilde{B}_{\tau'}^{(1)}$ and the delay spread $\tilde{B}_{\tau'}^{(2)}$ are defined by the first moment of the PDP $\tilde{p}_{\tau'}(\tau')$ and the square root of the second central moment of the PDP $\tilde{p}_{\tau'}(\tau')$, respectively. According to [17, Eqs. (7.152) and (7.153)], the average delay $\tilde{B}_{\tau'}^{(1)}$ and the delay spread $\tilde{B}_{\tau'}^{(2)}$ of the SOCUS channel simulation model are given by

$$\tilde{B}_{\tau'}^{(1)} = \frac{\sum_{l=0}^{L-1} \sum_{n=1}^{N_l} c_{n,l}^2 \tau_l'}{\sum_{l=0}^{L-1} \sum_{n=1}^{N_l} c_{n,l}^2} \tag{6}$$

and

$$\tilde{B}_{\tau'}^{(2)} = \sqrt{\frac{\sum_{l=0}^{L-1} \sum_{n=1}^{N_l} (c_{n,l} \tau_l')^2}{\sum_{l=0}^{L-1} \sum_{n=1}^{N_l} c_{n,l}^2} - \left(\tilde{B}_{\tau'}^{(1)}\right)^2} \tag{7}$$

respectively. The coherence bandwidth $\tilde{B}_C$ of the channel simulator is approximately reciprocally proportional to the delay spread $\tilde{B}^{(2)}_{\tau'}$, i.e., $\tilde{B}_C \approx 1/\tilde{B}^{(2)}_{\tau'}$ [17, p. 350].

E. PDF of the Channel Envelope

In this section, we analyze the PDF $p_{|H|}(x)$ of the absolute value of the TVCTF $|\tilde{H}(f', t)|$. Following the analytics in [17, Sect. (4.5.2)], it can be shown that the PDF of the envelope process $|\tilde{H}(f', t)| = |\sum_{l=0}^{L-1} \sum_{n=1}^{N_l} \tilde{\mu}_{n,l}(t) e^{-j2\pi f' \tau'_l}|$ of the SOCUS channel simulator is completely determined by the number of cisoids $L \times N_l$ and the choice of the gains $c_{n,l}$ according to

$$\tilde{p}_{|H|}(x) = (2\pi)^2 x \int_0^\infty \left[\prod_{l=0}^{L-l} \prod_{n=1}^{N_l} J_0(2\pi |c_{n,l}| y) \right] J_0(2\pi x y) y dy \tag{8}$$

where $J_0(\cdot)$ denotes the zeroth-order Bessel function of the first kind.

III. The Utilized Parameter Computation Method

In this section, we briefly explain the parameter computation method used in this paper. For the parametrization of the channel simulator, the latest version of INLSA algorithm is used, as described in [9]. According to [9, Eq. (4)], the channel parameters are computed in L independent steps, each of which corresponds to the estimation of the parameters of the channel gain $\tilde{\mu}_l(t)$ by minimizing the following error norm

$$\varepsilon_l = |\check{\mu}_l(t) - \tilde{\mu}_l(t)| \qquad \forall\ l = 0,\ 1,\ \ldots,\ L-1 \tag{9}$$

where $\check{\mu}_l(t)$ is the lth channel gain of the measured TVCIR $\check{h}(\tau', t)$ at $\tau' = \tau'_l$, i.e., $\check{\mu}_l(t) = \check{h}(\tau'_l, t)$. To solve each of the L minimization problems formulated by (9), the authors of [9] proposed an iterative parameter computation method according to the following steps

- Step 1: Set the iteration index q to zero.
- Step 2: Select the initial values $c^{(0)}_{n,l}$, $f^{(0)}_{n,l}$, and $\theta^{(0)}_{n,l}$ for all $l = 0,\ 1,\ \ldots,\ L-1$ and $n = 1,\ 2,\ \ldots,\ N_l$.
- Step 3: Compute the auxiliary error function $y^{(q)}_{n,l}(t_m)$ as

$$y^{(q)}_{n,l}(t_m) = \check{\mu}_l(t_m) - \sum_{p=1, p\neq n}^{N_l} c^{(q)}_{p,l} e^{j(2\pi f^{(q)}_{p,l} t + \theta^{(q)}_{p,l})} \tag{10}$$

where $t_m = m\Delta t$ ($m = 0,\ 1,\ \ldots,\ M-1$) is the discrete time, and Δt is the measurement time sampling interval.

- Step 4: Determine the value of gain $c^{(q+1)}_{n,l}$ as follows

$$c^{(q+1)}_{n,l} = \frac{\mathrm{Re}\left\{\mathbf{y}^{(q)}_{n,l}\right\}^T \mathrm{Re}\left\{\mathbf{s}^{(q)}_{n,l}\right\} + \mathrm{Im}\left\{\mathbf{y}^{(q)}_{n,l}\right\}^T \mathrm{Im}\left\{\mathbf{s}^{(q)}_{n,l}\right\}}{\left(\mathbf{s}^{(q)}_{n,l}\right)^H \mathbf{s}^{(q)}_{n,l}} \tag{11}$$

where the column vectors $\mathbf{y}^{(q)}_{n,l}$ and $\mathbf{s}^{(q)}_{n,l}$ contain the stacked values of $y^{(q)}_{n,l}(t_m)$ and the exponential function $e^{j(2\pi f^{(q)}_{n,l} t + \theta^{(q)}_{n,l})}$, respectively. The operators $\{\cdot\}^T$ and $\{\cdot\}^H$ denote the transpose and the complex-conjugate transpose, respectively.

- Step 5: The Doppler frequency $f^{(q+1)}_{n,l}$ is obtained as follows

$$f^{(q+1)}_{n,l} = \arg\min_{f_{n,l}} \left\| \mathbf{y}^{(q)}_{n,l} - c^{(q+1)}_{n,l} \mathbf{s}^{(q)}_{n,l} \right\|_2^2. \tag{12}$$

- Step 6: The phase $\theta^{(q+1)}_{n,l}$ can be computed as

$$\theta^{(q+1)}_{n,l} = \arg\min_{\theta_{n,l}} \left\| \mathbf{y}^{(q)}_{n,l} - c^{(q+1)}_{n,l} \mathbf{s}^{(q)}_{n,l} \right\|_2^2. \tag{13}$$

The parameter computation procedure defined in Steps 3–6 is applied to each of the N_l paths, which corresponds to one iteration. The error norm ε_l in (9) is re-evaluated at the end of each iteration. In case of a noticeable change of ε_l, the iteration index q is increased by one, i.e., $q + 1 \rightarrow\ q$. The parameter computation procedure is carried out again starting from Step 3. The iteration algorithm is terminated if the relative change in the error norm ε_l is below a given threshold ϵ, i.e, $|\varepsilon^{(q+1)}_l - \varepsilon^{(q)}_l| < \epsilon$.

IV. Measurement Scenario

The experimental data was collected near the New Jersey shore in May 2009 by a team from the School of Electrical and Computer Engineering at the Georgia Institute of Technology. The water depth was about 80 m and the sediment was a silty clay. Two stationary vertical arrays were placed near the water column. The stationary vertical transmit array named ASRA was about 45.57 m below the surface float ($y^T_1 = 45.57$ m). However, only the highest hydrophone had been used for transmission. On the receiver side, an acoustic communications and data storage (ACDS) stationary array named ACDS3, equipped with eight hydrophones with an aperture of 2.06 m was used. The first hydrophone was at 41.96 m depth ($y^R_1 = 41.96$ m), and all other hydrophones were lower with a hydrophone spacing of 2.06 m. The ACDS3 receiver was 1500 m away from the ASRA transmitter. The speed of sound in that shallow water environment was about 1440 m/s and the weather was rainy and windy. The 1×8 single-input multiple-output (SIMO) channel measurements were performed at a carrier frequency of 17 kHz and a signal bandwidth of 4 kHz. The signal, used for channel sounding, was an inverse linear frequency modulation (LFM) chirp. Fig. 1 demonstrates the measurement configuration of the underwater propagation scenario.

V. Measurement Results

In this section, we analyse the measured data by computing the statistical properties of the measured UWA channel.

A. Measured TVCIR

We start from the TVCIR $\check{h}(\tau', t)$ which has been measured by $M = 20$ samples in the time domain over a time range of $T_{\text{mes}} = 8$ s. Hence, the sampling interval Δt in the time domain is $\Delta t = T_{\text{mes}}/M = 0.4$ s. In the delay domain, the measurement equipment allows a path resolution of $\Delta\tau' = 0.125$ ms. The number of samples in the delay domain was equal to $L = 90$. In other words, one can say that the TVCIR

$\check{h}(\tau', t)$ has been measured at discrete time instances $t_m = m\Delta t \in [0, T_{\text{mes}}),\ m = 0,\ 1,\ \ldots,\ M-1$, and at the discrete delay interval $\tau'_l = l\Delta\tau',\ l = 0,\ 1,\ \ldots,\ L-1$. Consequently, the TVCIR $\check{h}(\tau', t)$ can be represented as a discrete TVCIR $\check{h}[\tau'_l, t_m]$.

B. Measured TVCTF

The discrete TVCTF $\check{H}[f'_k, t_m]$ can be obtained by computing the discrete Fourier transform of the TVCIR $\check{h}[\tau'_l, t_m]$ with respect to τ', which results in

$$\check{H}[f'_k, t_m] \quad = \sum_{l=0}^{L-1} \check{h}[\tau'_l, t_m]\ e^{-j2\pi\tau'_l f'_k} \tag{14}$$

where the discrete frequencies f'_k are given by $f'_k = -B/2 + k\Delta f' \in [-B/2, B/2),\ k = 0,\ 1,\ \ldots,\ K-1$ and B stands for the measurement bandwidth.

C. Measured TFCF

The discrete TFCF $\check{r}_{HH}[\nu'_p, \tau_q]$ can be obtained from the discrete TVCTF $\check{H}[f'_k, t_m]$ and can be expressed by

$$\check{r}_{HH}[\nu', \tau] = \frac{1}{MK} \sum_{k=0}^{K-1} \sum_{m=0}^{M-1} \check{H}[f'_k, t_m]\, \check{H}^*[f'_k + \nu', t_m + \tau] \tag{15}$$

where the discrete frequency separation ν' and the discrete time separation τ are given by $\nu' = 0,\ \Delta f', \ldots,\ (K-1)\,\Delta f'$, and $\tau = 0,\ \Delta t,\ \ldots,\ (M-1)\,\Delta t$, respectively.

D. Measured PDP

The discrete PDP $\check{p}_{\tau'}[\tau'_l]$ of the measurement data can be computed from the discrete TVCIR $\check{h}[\tau'_l, t_m]$ as follows

$$\check{p}_{\tau'}[\tau'_l] = \frac{1}{M} \sum_{m=0}^{M-1} |\check{h}[\tau'_l, t_m]|^2. \tag{16}$$

The average delay $\check{B}^{(1)}_{\tau'}$ is defined by the first moment of the PDP $\check{p}_{\tau'}[\tau'_l]$, and the delay spread $\check{B}^{(2)}_{\tau'}$ is defined by the square root of the second central moment of the PDP $\check{p}_{\tau'}[\tau'_l]$ which are given by [17, p. 348]

$$\check{B}^{(1)}_{\tau'} = \frac{\sum_{l=0}^{L-1} \check{p}_{\tau'}[\tau'_l]\ \tau'_l}{\sum_{l=0}^{L-1} \check{p}_{\tau'}[\tau'_l]} \tag{17}$$

and

$$\check{B}^{(2)}_{\tau'} = \sqrt{\frac{\sum_{l=0}^{L-1} \check{p}_{\tau'}[\tau'_l]\ {\tau'_l}^2}{\sum_{l=0}^{L-1} \check{p}_{\tau'}[\tau'_l]} - \left(\check{B}^{(1)}_{\tau'}\right)^2} \tag{18}$$

respectively. As mentioned in Section II-D, the coherence bandwidth $\check{B}_c$ of the measured channel can be obtained from the channel delay spread $\check{B}^{(2)}_{\tau'}$, which is determined by $\check{B}_C \approx 1/\check{B}^{(2)}_{\tau'}$.

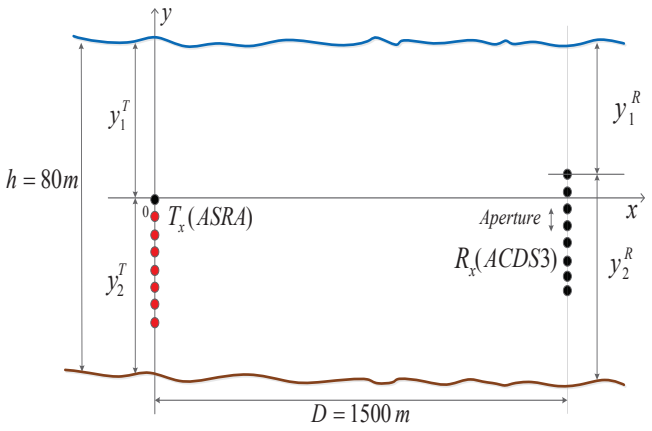

Fig. 1. The measurement configuration of the experiment for SIMO fixed-to-fixed (F2F) communication.

E. PDF of the Measured Channel Envelope

The PDF $\check{p}_{|H|}(x)$ of the measured channel envelope $|\check{H}(f', t)|$ can be obtained first by using the command *hist* in MATLAB®, which creates a histogram containing a number of equally spaced bins. Then, the histogram is normalized by dividing the number of events in each bin by the total number of events. The candidate distributions can then be fitted to the obtained PDF $\check{p}_{|H|}(x)$ of the measured channel envelope by means of the command *fitdist*.

VI. Numerical Results

In this section, we illustrate and verify the simulation results presented in the previous sections. For brevity, we focus here only on the single-input single-output (SISO) case. The performance of the channel simulator has been compared with that of the measured channel by analyzing the TVCIR and the statistical properties, including the TFCF, PDP, and the PDF of the channel envelope. After implementing the INLSA algorithm in MATLAB® and determining the UWA simulation model parameter set $\mathcal{P} = \{N_l, c_{n,l}, f_{n,l}, \theta_{n,l}\}$, we are able to compute the channel gains $\tilde{\mu}_l(t)$. The TVCIR $\tilde{h}(\tau', t)$ of the simulation model can be computed by taking into account that the corresponding propagation delay τ'_l of each channel gain $\tilde{\mu}_l(t)$ and the number of the Paths L are obtained directly from the measurement data.

Figs. 2 and 3 show the absolute value of the baseband measurement TVCIR $|\check{h}(\tau', t)|$ and the resulting TVCIR $|\tilde{h}(\tau', t)|$ of the simulation model, represented in (1), respectively. As can be seen, there is an excellent match between these two figures. This excellent match can be expected for other statistical properties of the UWA channel. Fig. 4 depicts the absolute value of the normalized TFCF $|\check{r}_{HH}(\nu', \tau)|$ of the measured channel. The absolute value of the normalized TFCF $|\tilde{r}_{HH}(\nu', \tau)|$ of the simulation model is shown in Fig. 5. From the inspection of Figs. 4 and 5, we can conclude that the TFCF of the simulation model is well fitted to that of the measurement data.

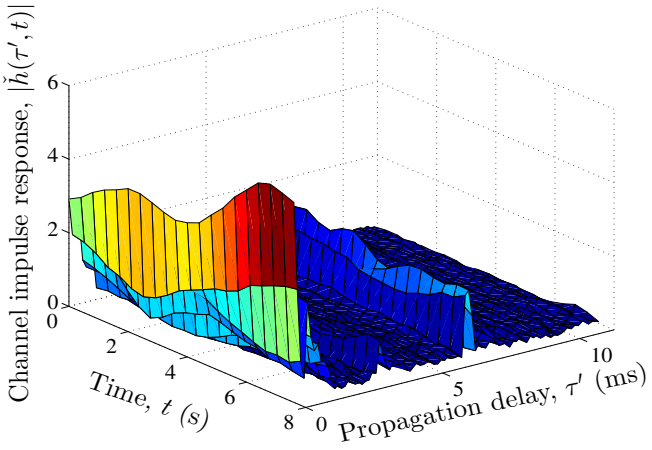

Fig. 2. Absolute value of the TVCIR $|\check{h}(\tau', t)|$ of the measured UWA channel.

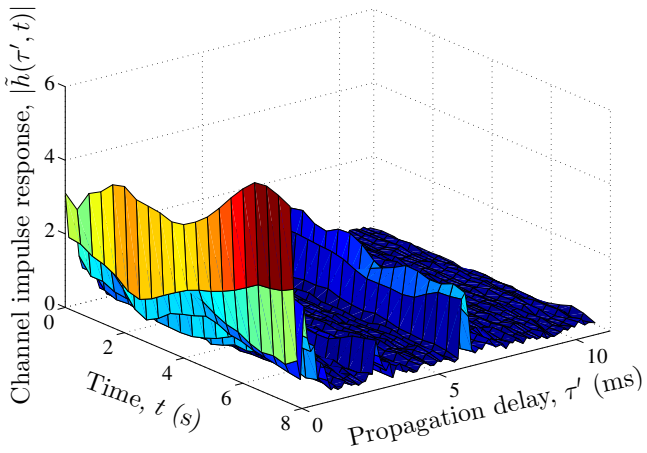

Fig. 3. Absolute value of the TVCIR $|\tilde{h}(\tau', t)|$ of the simulation model.

Fig. 6 depicts a comparison between the PDP $\check{p}_{\tau'}(\tau')$ of the measurement data and the corresponding PDP $\tilde{p}_{\tau'}(\tau')$ of the simulation model designed by using the INLSA algorithm. As can be seen, a good match can be achieved between the measurement data and the simulation model. Table I shows the characteristic quantities of the UWA channel obtained from the measurement data and the simulation model. With reference to Table I, there is a good match between the values obtained from the real-world data and the simulation model by using the INLSA parameter computation method. According to the simulation results, the value of the coherence bandwidth is about 420Hz, which is very small compared to terrestrial wireless channels. This small value is caused by the large value of the UWA channel delay spread, which is common for UWA channels.

Fig. 7 illustrates a comparison between the channel envelope PDF by using the approaches represented in Sections II-E and V-E. The results show that there is a good fitting between the channel envelope PDF of the measurement data provided by numerical computations and that of the analytical results represented in (8). We can also observe that all distributions follow the Rayleigh distribution.

VII. Conclusion

In this paper, we have used the latest version of the INLSA algorithm for designing measurement-based UWA channel simulators. The algorithm has been applied to UWA measurement data to estimate the parameters of the channel simulator. The TVCIR, TFCF, PDP, and the channel envelope distribution of the channel simulator have been matched to corresponding quantities of the measured channel. It has been shown that the INLSA algorithm precisely estimates the channel model parameters and provides an excellent fitting to measured UWA channels. We have also shown that the distribution of the UWA channel envelope follows closely the Rayleigh distribution.

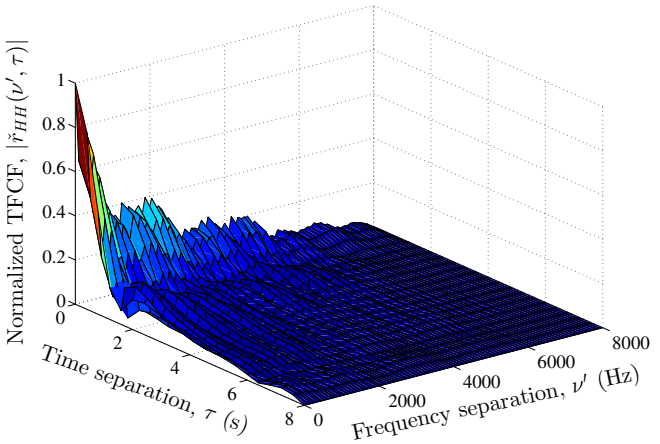

Fig. 4. Absolute value of the normalized TFCF $|\check{r}_{HH}(\nu', \tau)|$ of the measured UWA channel.

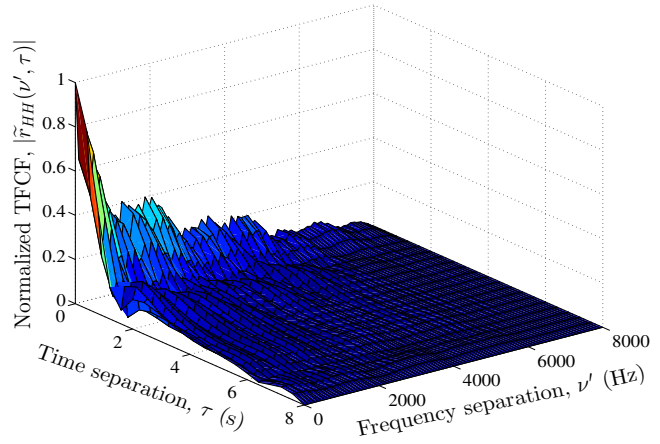

Fig. 5. Absolute value of the normalized TFCF $|\tilde{r}_{HH}(\nu', \tau)|$ of the simulation model.

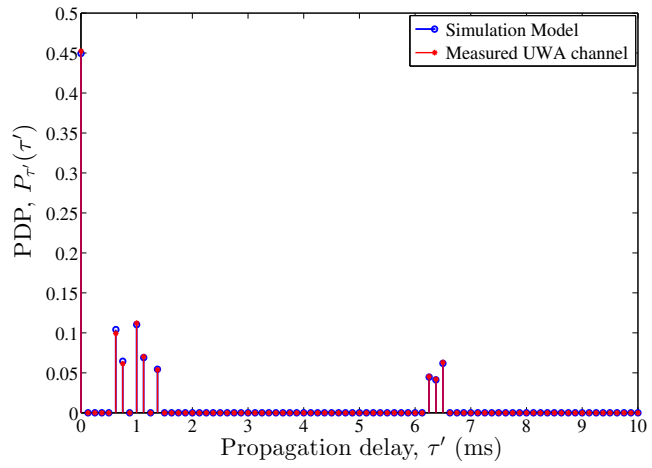

Fig. 6. The PDP $\check{p}_{\tau'}(\tau')$ of the UWA measured channel compared to the PDP $\tilde{p}_{\tau'}(\tau')$ of the simulation model.

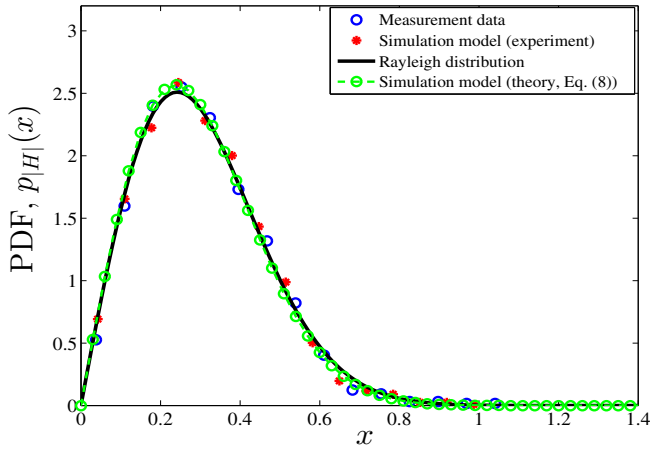

Fig. 7. The PDF of the UWA channel envelope .

TABLE I
CHARACTERISTIC QUANTITIES OF THE UWA CHANNEL.

R	Channel parameter	Measured channel	Simulation model
1	Average delay $B^{(1)}_{\tau'}$	1.5 ms	1.46 ms
2	Delay spread $B^{(2)}_{\tau'}$	2.4 ms	2.35 ms
3	Coherence bandwidth B_C	$\approx$ 416 Hz	$\approx$ 424 Hz

REFERENCES

[1] A. G. Zajić, "Statistical modeling of MIMO mobile-to-mobile underwater channels," *IEEE Trans. Veh. Technol.*, vol. 60, no. 4, pp. 1337–1351, May 2011.

[2] P. Qarabaqi and M. Stojanovic, "Statistical characterization and computationally efficient modeling of a class of underwater acoustic communication channels," *IEEE J. Ocean. Eng.*, vol. 38, no. 4, pp. 701–717, Oct. 2013.

[3] M. Naderi, M. Pätzold, and A. G. Zajić, "A geometry-based channel model for shallow underwater acoustic channels under rough surface and bottom scattering conditions," in *Proc. 5th Int. Conf. on Communications and Electronics, ICCE 2014, Da Nang, Vietnam*, July/Aug. 2014, pp. 112–117.

[4] J. Fuhl, J.-P. Rossi, and E. Bonek, "High-resolution 3-D direction-of-arrival determination for urban mobile radio," *IEEE Antennas Propag. Mag.*, vol. 45, no. 4, pp. 672–682, Apr. 1997.

[5] B. H. Fleury, M. Tschudin, R. Heddergott, D. Dahlhaus, and K. I. Pedersen, "Channel parameter estimation in mobile radio environments using the SAGE algorithm," *IEEE J. on Selected Areas in Communications*, vol. 17, no. 3, pp. 434–450, Mar. 1999.

[6] D. Umansky and M. Pätzold, "Design of measurement-based wideband mobile radio channel simulators," in *Proc. 4th IEEE Int. Symp. on Wireless Communication Systems, ISWCS 2007, Trondheim, Norway*, Oct. 2007, pp. 229–235.

[7] A. Fayziyev and M. Pätzold, "An improved iterative nonlinear least square approximation method for the design of measurement-based wideband mobile radio channel simulators," in *Proc. Int. Conf. on Advanced Technologies for Communications, ATC 2011, Danang, Vietnam*, Aug. 2011, pp. 106–111.

[8] A. Fayziyev and M. Pätzold, "An improved iterative nonlinear least square approximation method for the design of SISO wideband mobile radio channel simulators," *REV J. on Electronics and Communications*, vol. 2, no. 1–2, pp. 19–25, Jan.-June 2012.

[9] A. Fayziyev, M. Pätzold, E. Masson, Y. Cocheril, and M. Berbineau, "A measurement-based channel model for vehicular communications in tunnels," in *Proc. IEEE Wireless Communications and Networking Conf., WCNC 2014, Istanbul, Turkey*, Apr. 2014, pp. 128–133.

[10] A. Fayziyev and M. Pätzold, "The performance of the INLSA in comparison with the SAGE and ESPRIT algorithms," in *Proc. IEEE Advanced Technologies for Communications, ATC 2014, Hanoi, Vietnam*, Oct. 2014, in press.

[11] F.-X. Socheleau, J.-M. Passerieux, and C. Laot, "Characterisation of time-varying underwater acoustic communication channel with application to channel capacity," in *Proc. Underwater Acoustic Measurements Conf., Nafplion, Greece*, June 2009.

[12] R. Galvin and R. F. W. Coats, "A stochastic underwater acoustic channel model," in *Proc. OCEANS '96. MTS/IEEE. Prospects for the 21st Century.*, Sep. 1996, vol. 1, pp. 203–210.

[13] P. Qarabaqi and M. Stojanovic, "Statistical modeling of a shallow water acoustic communication channel," in *Proc. Underwater Acoustic Measurements Conf., Nafplion, Greece*, June 2009, pp. 1341–1350.

[14] A. Radosevic, J. G. Proakis, and M. Stojanovic, "Statistical characterization and capacity of shallow water acoustic channels," in *Proc. IEEE OCEANS 2009 - EUROPE*, May 2009, pp. 1–8.

[15] B. Tomasi, P. Casari, L. Badia, and M. Zorzi, "A study of incremental redundancy hybrid ARQ over Markov channel models derived from experimental data," in *Proc. WUWNet, Woods Hole, Massachusetts, USA*, Sep. 2010, pp. 1–8.

[16] J. Zhang, J. Cross, and Y. R. Zheng, "Statistical channel modeling of wireless shallow water acoustic communications from experiment data," in *Proc. Military Communication Conf., MILCOM 2010*, Oct. 2010, pp. 2412–2416.

[17] M. Pätzold, *Mobile Fading Channels*, Chichester: John Wiley & Sons, 2nd edition, 2011.